Digital reconstruction of teeth using near-infrared light

Keith Angelino[1], Gregory Yauney[1], Aman Rana[1], David Edlund[2] and Pratik Shah[1†]

***Abstract*— Cone beam computed tomography has demonstrated value by offering enhanced conceptualization of features of teeth in the 3D space. However, these systems require higher effective radiation doses to image teeth. Previous research from our group has used non-ionizing near-infrared (NIR) light for diagnosing demineralization and caries in human tooth enamel. However, use of safe NIR radiation for rapid, 3D imaging of tooth anatomy has not been described previously. Here we describe a optical setup to rapidly laser scan teeth ex vivo using 1310nm NIR laser diode. We also detail a novel process that uses laser scanning to create stacks of images of extracted teeth, and construct highly accurate 3D models. Our 3D reconstructive models offer promising starting points to recover anatomical details using pixel intensities within these images as projection data to diagnose carious lesions, and can assist in providing rapid and affordable technology-enabled early caries screenings to patients.**

I. Introduction

NIR light is a promising research method for assessing dental structures without using ionizing radiation. Tooth enamel has a higher translucency to NIR light compared to the visible spectrum, with a reported peak opacity at 1310nm [1]–[3]. Tooth dentin scatters much more than enamel, but retains some translucency [4]. Demineralization and caries scatter NIR light and are highly visible when compared against healthy enamel. Transillumination of teeth using NIR light is a promising research method for assessing dental structures without using ionizing radiation [1], [3]. Imaging teeth using in a NIR reflectance configuration has also shown promise for detecting caries in certain settings, but may be constrained to latter portions of the NIR spectrum [5]. In our own studies, we investigated the value proposition of NIR dental imaging and state its potential as a screening tool prior to radiography by construction and validation of low-cost, point-of-care near-infrared imaging devices to diagnose dental caries, cracks, and demineralization [6], [7]. We have open-sourced the construction and the algorithm of porphyrin imaging device, and a cell-phone clip that can be used on a mobile phone camera [8].

Imaging technologies that generate tomography and 3D models of hard dental tissues have proven to be irreplaceable in value [9]–[11]. Cone beam computed tomography (CBCT) is a three-dimensional form of radiography and has seen rapid adoption in recent years within dentistry [12]. CBCT allows for the digital reconstruction of a patients teeth and jaw; however, CBCT generally requires a comparatively higher dosage of X-rays than two-dimensional radiographs [13], [14]. CBCT imaging is also limited by the resolution of its voxel size, which can lead to circumstantial shortcomings when compared to other imaging methods [15]–[17]. There remains a need to develop the framework for a method that can reconstruct oral anatomy without the use of ionizing radiation, and to also computationally compensate for optical phenomenon that hinder feature extraction.

To our knowledge, there has been no prior method that utilizes NIR light in conjunction with an imaging scheme to reconstruct and resolve dental structures on the macro-scale. While various other techniques which produce tomography in certain applications exist [18]–[20], the most widely accepted framework behind conventional tomography are X-rays and the Radon transform. In this manner, cross-sectional images can be derived from projection data. This is highly applicable in medicine and also the operating principle behind the CT scan and its derivative, CBCT. In this report we detail a novel reconstruction process for rapid laser-scanning of extracted teeth on the bench to create stacks of images and use these for 3D modeling. Using pixel intensities within these images as projection data, these images and models can be further used for visualizing the internal anatomy of the tooth.. Our method is adaptable to other applications that may benefit from a bench NIR reconstruction process.

II. Methods

Sample collection and clinical evaluations: Five extracted sample teeth were obtained as remnants from patient clinical procedures (no identifying patient data was recorded) (Figure 1). Samples were debrided of residual tissue, washed, and allowed to air dry. A clinician then evaluated each sample in normal room lighting conditions. Four teeth had unique carious features (evidenced by radiolucency on 2D radiograph) either in the dentino-enamel junction (DEJ), enamel or the dentin (Figure 1). A healthy fifth tooth served as a control.

Radiographic imaging: A Planmeca ProMax 3D imaging system (Planmeca, Helsinki, Finland) was used for 3D radiography of each sample. Samples were mounted upright in wax during radiography. 3D radiographs were used to confirm the location of the carious lesions on selected teeth (Figure 1). A Heliodent X-ray system (Sirona Dental Systems, Bensheim, Germany) coupled with a Kodak RVG 6100 intraoral sensor (Carestream Dental, Atlanta, Georgia, United States) granted 2D radiographic images of each tooth. A Planmeca ProMax 3D imaging system (Planmeca, Helsinki, Finland) was used for 3D radiography. In both setups, teeth

[1]MIT Media Lab, Massachusetts Institute of Technology, Cambridge, MA, USA {gyauney, arana, pjavia, pratiks}@mit.edu
[2]Hampden Dental Care, Lakewood, CO, USA davidedlund777@gmail.com
[†]Corresponding Author

978-1-5386-1311-5/19/$31.00 ©2019 IEEE

were mounted upright in wax during radiography. A clinician then evaluated carious features in both the 2D and 3D radiographic sets.

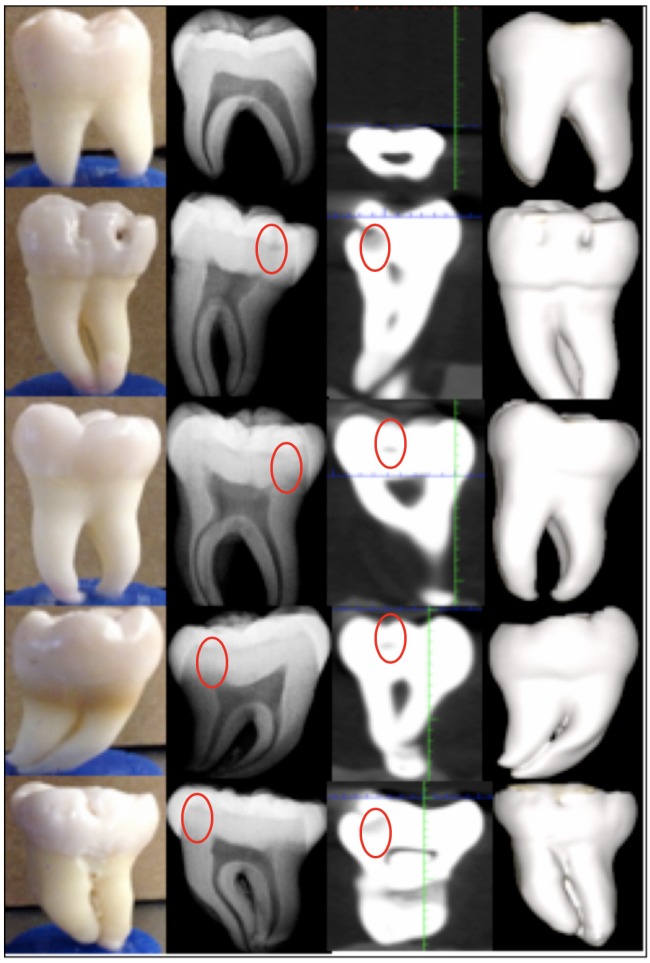

Fig. 1: Imaging of selected teeth. Whitelight (1^{st} column), 2D radiographs (2^{nd} column), cone-beam computed tomography (3^{rd} column) and stereo lithography images (4^{th} column). Red circles indicate approximate locations of caries. First row of images show healthy tooth.

Clinical evaluation: A dentist examined all teeth and 2D and 3D radiograph and identified specific clinical features of diagnostic value. Each clinical feature was carefully measured using MATLAB software (MathWorks, Natick, MA) to calculate its area on the 2D and 3D radiographs. Additionally, setting the stage height=0 on axis of rotation, approximate location of caries (mm) was calculated for each tooth that was imaged for comparison with reconstructed NIR tomography images.

Optical setup: A laser beam was generated using a 1310 nm laser diode (Thorlabs, Inc., Newton, New Jersey, USA) and an accompanying driver (Figure 2). The beam was focused using a lens collimation package, and beam artifacts were removed with an iris. The beam passed through a custom rotating diffuser system to reduce laser speckle, and then a 150 m aperture to reduce its spot size. The beam

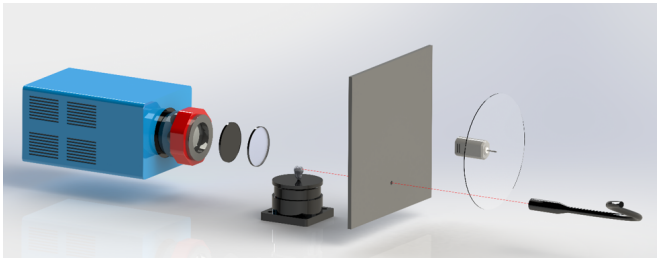

Fig. 2: NIR transillumination: The tooth was placed in front of a camera and transilluminated by a 1310nm laser and imaged with a laser beam directed from the side passing through the diffuser and the polarizer to the middle of the tooth.

was then directed orthogonally to the center axis of a rotary stage (Thorlabs, Inc., Newton, New Jersey, USA). A TriWave InGaAs infrared camera (NoblePeak Vision Corporation, Wakefield, Massachusetts, USA) was positioned such that the rotary stage was centered in-frame. A 1310 nm bandpass filter and polarizer were mounted on the camera lens (Thorlabs, Inc., Newton, New Jersey, USA); the filter limited capture to a narrow spectrum of light (Figure 2). Each sample was attached to an insert that could be precisely and repeatedly placed upon the center axis of the rotary stage. Because the laser beam was positioned to intersect with the center axis of the rotary stage, each sample can be illuminated at a point on its approximate mid-line. By stepping the laser dots up the midline, sets of vertical illumination images can be captured. The distance between each vertical step point was 1 mm, staring at the level of the rotary stage. At each vertical step point, the rotary stage would complete a full rotation, with the infrared camera attaining an image every three degrees. Vertical stepping of the laser proceeded for the entire height of each sample. Because of the non-homogeneity of the tooth samples, the camera integration time was adjusted between step points. For example, a thicker center section with a large volume of dentin requires a longer integration time than a thinner enamel section. Integration times were also picked to avoid pixel saturation in images. Image collection was performed with the polarizer rotated to its minimum and maximum polarization angle, resulting in dual stacks of polarized and unpolarized images for each sample.

Image capture: Automation of the image and stage were done to save labor and time. Both were done via a MATLAB script, which ran on a computer that was connected to the stage and TriWave camera. Stage control was accomplished directly via MATLAB input, but the TriWave image capture was performed via robot mouse clicks. The mouse was commanded to screen pixel coordinates and told to click, release, or wait (to allow for the image to save or stage to rotate). In the TriWave camera settings (Control dialogue), Gain was set to 0. Integration time served as the exposure adjustment mechanism in order to avoid pixel saturation. Integration time was adjusted per tooth to avoid saturation.

III. Results

Preprocessing: While the image stacks provided pixel intensities at various illumination modes for the samples, they need to be correlated to 3D surface points. Stereolithography (STL) models containing sample surface data were generated from each DICOM using MATLAB. While a 3D model of each tooth could have been obtained via a conventional 3D scanner, we chose to generate them using the DICOM out of convenience; these STLs contain surface data can be used to model the tooth shape. The STL models were placed in a virtual recreation of the optical setup in MATLAB to simulate the incidence of the laser to each sample. The virtual setup included real-life measurements of bench components and perspective adjustments via calibration images; this aids in the alignment of the rotary stage axis to the virtual axis in the image stacks, ultimately improving the projection of pixel data onto the 3D model of the sample. The end result is a 3D model array with complementary surface pixel intensity data.

Reconstruction: We used stacks of 2D NIR image collected using our optical bench setup for creating a 3D model. For each tooth, we captured sets of 120 near-infrared images at 1350 nm taken at 3-degree intervals on a rotating stage, where a laser in a different vertical position illuminated each image set. Real world distances between the stage, the laser, the camera, and calibration points were measured. We then oriented a 3D model of the tooth, captured with CBCT, with respect to the camera and the calibration points. The centroids of all the faces in a mesh were located to approximate the surface of the tooth, and these centroids were used for further operations on the 3D points. Random sample consensus method (RANSAC) was used to solve for the homography matrix, by matching the 2D and 3D coordinates of the calibration points, that best transformed the points in the 3D scene into the coordinate space of the near-IR images [21]. For each angle of the stage, we rotated the 3D model a corresponding amount and find the subset of the 3D points that are visible from that angle by using ray casting to check if each point was occluded from the camera by the mesh [22]. We then transformed the 3D points into the space of the image by multiplying them by the homography matrix. Interpolation of the intensity from the image for each transformed 3D point and mapping it back to the corresponding point in the 3D scene was the last step. This entire process was repeated for all angles and each laser position.

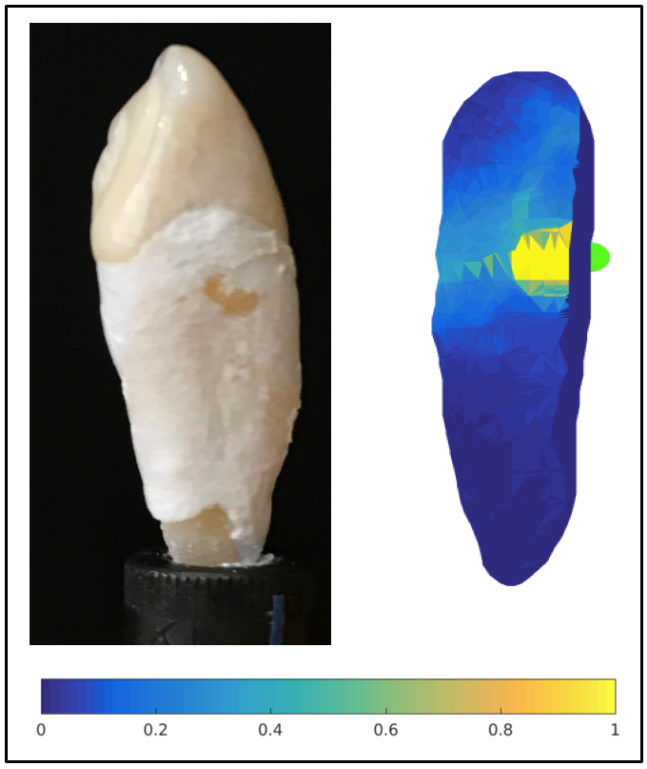

Fig. 3: NIR 3D modeling of teeth: Left: whitelight photograph; Right: 3D NIR model of the tooth projected on stereolithography file. Heat map indicates intensity of photons on the tooth. Green indicates point-of-impact of laser beam.

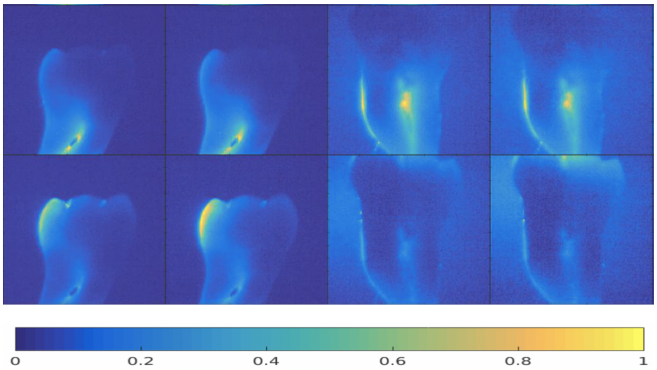

Fig. 4: NIR 3D modeling of multiple teeth. 3D NIR model of multiple teeth projected on stereolithography file. Heat map indicates intensity of photons on the tooth.

We were also able to find the projection of the laser onto the 3D tooth model, identifying the point where the laser hit the tooth for each angle and laser position during collection of data. The angle-varying intensity information showing each centroid's interpolated intensity on its entire corresponding face and cycle through each angle and laser position is shown in one such 3D model of an extracted canine (Figure 3). While individual image stacks provide pixel intensities at various illumination modes for the samples, they were correlated to 3D surface points in order to reconstruct an interior geometry. STL models containing sample surface data was generated from DICOM files of each tooth using MATLAB. Each of the constructed 3D models was carefully compared to the STL file generated by the CBCT system for accuracy (Figure 4). The ability to reconstruct these 3D models thus is an important accomplishment to start recovering tomographic information of teeth.

IV. Discussion

Diagnosis and classification of dental caries today are almost entirely based on visual clinical assessments and 2D radiographs. In addition, some indices recommend tactile examination via probing to be performed in conjunction with visual examination. Previous reports have shown inconclusive results with regard to tactile examination performance, and a lack of information concerning the examiners training and manner of using the explorer [23]. The International and Caries Detection Assessment System, Nyvads, Decayed Missing Filled are some of the methods used to classify caries by severity based on visual assessment and a probe. These approaches are time-consuming, subjective, manual and often only identify diseases visible to the human eye [24], [25]. There is an urgent need to develop valid and reliable methods for caries risk assessment that are based on best evidence for prediction and disease management.

NIR is preferred for caries detection compared to visible light imaging because it exhibits low absorption by stain and deeper penetration into teeth [26]. It is also noninvasive, noncontact, and stain insensitive. Evaluated against 2D radiographs, NIR imaging has been shown to capture a higher level of detail of demineralized and carious enamel [26], [27]. Researchers have imaged teeth across the NIR range and into the short-wavelength infrared range [28], [28], [29]. As current CCD and CMOS technologies have sensitivities that extend into the NIR range [30], [31], some NIR imaging is realizable with Indium gallium arsenide (InGaAs) infrared cameras operating on wavelengths of 0.9-1.7 m such as the one used in this study [32]. A small selection of market devices utilizing NIR light are available for purchase, such as the DEXIS CariVuTM (DEXIS, LLC, Hatfield, PA) and Drr Dentals VistaCam iX (Drr Dental, Bietigheim-Bissingen, Germany). These lack accurate, clinically validated image-processing algorithms, are expensive and only capture 2D images, precluding their use by dentists.

In prior work [5], [33] and in our own investigations in this study, we found that tooth hydration had a substantial impact on the appearance of the tooth in images. Preliminary tests revealed that a fully-hydrated tooth could appear substantially different if left to air-dry for only a few minutes. While our imaging mode favored hydrated teeth for greater imaging depth and improved lesion contrast, there was no practical way by which the teeth could be consistently rehydrated, especially during the automated image acquisition periods. We therefore chose to image our teeth in dry conditions. Oversaturation of pixels within images signifies lost data in our research, so we selectively altered the camera exposure to avoid saturation from the laser light. However, optical differences between the enamel and dentin and the difference in material thicknesses in the tooth resulted in images containing imbalanced contrasts. For instance, the high optical channeling of the enamel would cause it to appear saturated in images where the tooth was illuminated level to its centroid; however, when exposure was shortened to account for this, regions with thicker sections of dentin would be indistinguishable from background noise. We chose to avoid image saturation to acquire enamel anatomy at the sacrifice of reconstructing dentin anatomy closer to the root. To avoid this problem in the future, a possible solution could be to image at multiple exposures and obtain partial datasets from each, and combine the two resolved areas.

V. Conclusion

Technology that generates tomography and 3D models of hard dental tissues has proven to be irreplaceable in value. While advancements in CBCT provide this capability and enable dentists to draw more conclusive diagnoses, it comes with increasing the effective radiation dosage to the patient. Optical coherence tomography (OCT) and standard NIR methods may provide potential solutions here. We detail a reconstruction process for laser-scanning extracted teeth on the bench to create stacks of images, We also detail a novel process to construct highly accurate 3D models. Our 3D reconstructive models offer promising starting points to recover anatomical details using pixel intensities within these images as projection data to diagnose carious lesions, and can assist in providing rapid and affordable technology-enabled early caries screenings to patients. To our knowledge, this is the first description of rapid 3D reconstruction of human teeth using NIR laser diodes.

VI. Acknowledgements

The authors thank Guy Satat for his contributions to this research.

References

[1] R. S. Jones and D. Fried, "Attenuation of 1310-and 1550-nm laser light through sound dental enamel," in *Lasers in dentistry VIII*, vol. 4610. International Society for Optics and Photonics, 2002, pp. 187–191.

[2] C. M. Bühler, P. Ngaotheppitak, and D. Fried, "Imaging of occlusal dental caries (decay) with near-ir light at 1310-nm," *Optics Express*, vol. 13, no. 2, pp. 573–582, 2005.

[3] R. S. Jones, G. D. Huynh, G. C. Jones, and D. Fried, "Near-infrared transillumination at 1310-nm for the imaging of early dental decay," *Optics Express*, vol. 11, no. 18, pp. 2259–2265, 2003.

[4] D. Fried, R. E. Glena, J. D. Featherstone, and W. Seka, "Nature of light scattering in dental enamel and dentin at visible and near-infrared wavelengths," *Applied optics*, vol. 34, no. 7, pp. 1278–1285, 1995.

[5] S. Chung, D. Fried, M. Staninec, and C. L. Darling, "Multispectral near-ir reflectance and transillumination imaging of teeth," *Biomedical optics express*, vol. 2, no. 10, pp. 2804–2814, 2011.

[6] K. Angelino, D. A. Edlund, and P. Shah, "Near-infrared imaging for detecting caries and structural deformities in teeth," *IEEE journal of translational engineering in health and medicine*, vol. 5, pp. 2 300 107–2 300 107, 2017.

[7] K. Angelino, D. Edlund, G. Bhatia, S. Wu, and P. Shah, "Near-infrared transillumination guides administration of dental 2d radiography and cbct imaging," in *Bioinformatics and Bioengineering (BIBE), 2017 IEEE 17th International Conference on*. IEEE, 2017, pp. 327–333.

[8] K. Angelino, P. Shah, D. A. Edlund, M. Mohit, and G. Yauney, "Clinical validation and assessment of a modular fluorescent imaging system and algorithm for rapid detection and quantification of dental plaque," *BMC Oral Health*, vol. 17, no. 1, 2017. [Online]. Available: http://bit.ly/2rjwlYf.

[9] Z. Xuedong, *Dental caries: principles and management*. Springer, 2015.

[10] J. Souza, T. Boldieri, M. Diniz, J. Rodrigues, A. Lussi, and R. d. C. L. Cordeiro, "Traditional and novel methods for occlusal caries detection: performance on primary teeth," *Lasers in medical science*, vol. 28, no. 1, pp. 287–295, 2013.

[11] B. Vandenberghe, R. Jacobs, and H. Bosmans, "Modern dental imaging: a review of the current technology and clinical applications in dental practice," *European radiology*, vol. 20, no. 11, pp. 2637–2655, 2010.

[12] W. C. Scarfe and A. G. Farman, "What is cone-beam ct and how does it work?" *Dental Clinics of North America*, vol. 52, no. 4, pp. 707–730, 2008.

[13] G. Li, "Patient radiation dose and protection from cone-beam computed tomography," *Imaging science in dentistry*, vol. 43, no. 2, pp. 63–69, 2013.

[14] T. Okano and J. Sur, "Radiation dose and protection in dentistry," *Japanese Dental Science Review*, vol. 46, no. 2, pp. 112–121, 2010.

[15] S. Haghanifar, S. Yousefi, E. Moudi, F. Abesi, A. Bijani, A. A. Moghadamnia, and M. Nabahati, "Accuracy of densitometry of two cone beam computed tomography equipment in comparison with computed tomography," *Electronic physician*, vol. 9, no. 5, p. 4384, 2017.

[16] S. L. S. Melo, M. D. F. Belem, L. T. Prieto, C. P. M. Tabchoury, and F. Haiter-Neto, "Comparison of cone beam computed tomography and digital intraoral radiography performance in the detection of artificially induced recurrent caries-like lesions," *Oral surgery, oral medicine, oral pathology and oral radiology*, vol. 124, no. 3, pp. 306–314, 2017.

[17] M. M. Vidor, G. S. Liedke, M. P. Fontana, H. L. D. da Silveira, N. A. Arus, A. Lemos, and M. B. Vizzotto, "Is cone beam computed tomography accurate for postoperative evaluation of implants? an in vitro study," *Oral surgery, oral medicine, oral pathology and oral radiology*, vol. 124, no. 5, pp. 500–505, 2017.

[18] X. Ma, W. Xiao, and F. Pan, "Accuracy improvement in digital holographic microtomography by multiple numerical reconstructions," *Optics and Lasers in Engineering*, vol. 86, pp. 338–344, 2016.

[19] D. Pickens, R. Price, J. Patton, J. Erickson, F. Rollo, and A. Brill, "Focal-plane tomography image reconstruction," *IEEE Transactions on Nuclear Science*, vol. 27, no. 1, pp. 489–492, 1980.

[20] W. Krauze, A. Kuś, D. Śladowski, E. Skrzypek, and M. Kujawińska, "Reconstruction method for extended depth-of-field optical diffraction tomography," *Methods*, vol. 136, pp. 40–49, 2018.

[21] R. Szeliski, *Computer vision: algorithms and applications*. Springer Science & Business Media, 2010.

[22] J. F. Hughes, A. Van Dam, J. D. Foley, M. McGuire, S. K. Feiner, D. F. Sklar, and K. Akeley, *Computer graphics: principles and practice*. Pearson Education, 2014.

[23] M. M. Braga, F. M. Mendes, and K. R. Ekstrand, "Detection activity assessment and diagnosis of dental caries lesions," *Dental Clinics*, vol. 54, no. 3, pp. 479–493, 2010.

[24] M. Tellez, J. Gomez, I. Pretty, R. Ellwood, and A. Ismail, "Evidence on existing caries risk assessment systems: Are they predictive of future caries?" *Community Dentistry and Oral Epidemiology*, vol. 41, no. 1, pp. 67–78, feb 2013. [Online]. Available: http://doi.wiley.com/10.1111/cdoe.12003

[25] S. J. Carson, "Limited evidence for existing caries assessment systems," *Evidence-Based Dentistry*, vol. 14, no. 1, pp. 10–11, mar 2013. [Online]. Available: http://www.nature.com/doifinder/10.1038/sj.ebd.6400911

[26] D. Fried, M. Staninec, and C. L. Darling, "Near-Infrared Imaging of Dental Decay at 1310 nm AND NEW OPTICAL DIAGNOSTIC," Tech. Rep. 1, 2010. [Online]. Available: https://www.laserdentistry.org/uploads/files/members/jld/JLD{_}18.1/JLD{_}18{_}1{_}2{_}2010.pdf

[27] A. M. Maia, L. Karlsson, W. Margulis, and A. S. Gomes, "Evaluation of two imaging techniques: Near-infrared transillumination and dental radiographs for the detection of early approximal enamel caries," *Dentomaxillofacial Radiology*, vol. 40, no. 7, pp. 429–433, 2011. [Online]. Available: http://dmfr.birjournals.org

[28] S. Chung, D. Fried, M. Staninec, and C. L. Darling, "Multispectral near-IR reflectance and transillumination imaging of teeth," Tech. Rep. 10, 2011. [Online]. Available: https://www.osapublishing.org/boe/abstract.cfm?uri=boe-2-10-2804

[29] W. A. Fried, D. Fried, K. H. Chan, and C. L. Darling, "Imaging early demineralization on tooth occlusional surfaces with a high definition InGaAs camera," p. 85660I, 2013. [Online]. Available: http://proceedings.spiedigitallibrary.org/proceeding.aspx?doi=10.1117/12.2011015

[30] J. R. Janesick, *Scientific charge-coupled devices*. SPIE Press, 2001.

[31] J. Ohta, *Smart CMOS Image Sensors*. CRC Press, 2008.

[32] Grietens Bob, "InGaAs cameras allow broader NIR applications," 2009. [Online]. Available: http://optics.org/article/38064

[33] R. C. Lee, M. Staninec, O. Le, and D. Fried, "Infrared methods for assessment of the activity of natural enamel caries lesions," *IEEE Journal of Selected Topics in Quantum Electronics*, vol. 22, no. 3, pp. 102–110, 2016.